

No-Reference Image Quality Assessment by Hallucinating Pristine Features

Baoliang Chen, Lingyu Zhu, Chenqi Kong, Hanwei Zhu, Shiqi Wang, *Senior Member, IEEE* and Zhu Li, *Senior Member, IEEE*

Abstract—In this paper, we propose a no-reference (NR) image quality assessment (IQA) method via feature level pseudo-reference (PR) hallucination. The proposed quality assessment framework is rooted in the view that the perceptually meaningful features could be well exploited to characterize the visual quality, and the natural image statistical behaviors are exploited in an effort to deliver the accurate predictions. Herein, the PR features from the distorted images are learned by a mutual learning scheme with the pristine reference as the supervision, and the discriminative characteristics of PR features are further ensured with the triplet constraints. Given a distorted image for quality inference, the feature level disentanglement is performed with an invertible neural layer for final quality prediction, leading to the PR and the corresponding distortion features for comparison. The effectiveness of our proposed method is demonstrated on four popular IQA databases, and superior performance on cross-database evaluation also reveals the high generalization capability of our method. The implementation of our method is publicly available on <https://github.com/Baoliang93/FPR>.

Index Terms—Image quality assessment, no-reference, mutual learning, pseudo-reference feature

I. INTRODUCTION

IMAGE quality assessment (IQA), which aims to establish the quantitative connection between the input image and the corresponding perceptual quality, serves as a key component in a wide range of computer vision applications [1]–[3]. The typical full-reference (FR) IQA models resort to fidelity measurement in predicting image quality via measuring the deviation from its pristine-quality counterpart (reference). The pioneering studies date back to 1970’s and a series of visual fidelity measures have been investigated [4]. Recently, there has been a demonstrated success for developing the FR quality measures, including the Peak Signal-to-Noise Ratio (PSNR), Structural Similarity Index (SSIM) [5], Multiscale SSIM (MS-SSIM) [6], Visual Saliency-Induced Index (VSI) [7], Median Absolute Deviation (MAD) [8] and Visual Information Fidelity (VIF) [9]. Unfortunately, in the vast majority of practical applications, the reference images are usually absent or difficult

to obtain, leading to the exponential increase in the demand for no-reference (NR) IQA methods. Compared with FR-IQA, NR-IQA is a more challenging task due to the lack of pristine reference information.

In the literature, numerous NR-IQA methods have been proposed based on the hypothesis that natural scenes possess certain statistical properties. Thus, the quality can be assessed by measuring the deviation of the statistics between distorted and pristine images [10]–[12]. With the development of deep learning technologies, the image quality can be inferred by learning from the labeled image data [13]–[19]. However, such data driven based methods highly rely on the large-scale training samples. Recently, the free-energy based brain theory [20]–[23] provides a novel solution for NR-IQA from the Bayesian view. In particular, the free energy theory reveals that human visual system (HVS) may attempt to infer the reference signals to reduce the uncertainty of perceived visual signals by an internal inference model. Rooted in the widely accepted view that the intrinsic, perceptually-meaningful and learnable features could govern the image quality, in this work, we focus on the feature level reference information estimation for IQA. This method avoids the modeling of the image signal space of which the understanding is still quite limited. Herein, we propose to learn a new NR-IQA measure named **FPR**, by inferring the quality through **Feature-level Pseudo-Reference** information. The underlying design philosophy of our method is learning the quality-specific PR feature instead of the restoration-specific PR feature. Along this vein, we can get rid of the design of a specific network for PR image generation, which is still a very challenging task. Besides, a gated recurrent units (GRU) [24] aggregation strategy is proposed to aggregate the quality of each patch in the test image. The GRU network processes the image patches in order, and the long-term memory enjoyed by GRU can construct the long-dependency between each patch. To verify the performance of our method, we conduct both intra-database and cross-database experiments on four databases, including TID2013 [25], LIVE [26], CSIQ [8] and KADID-10k [27]. Experimental results have demonstrated the superior performance of our method over existing state-of-the-art models. The main contributions of this paper are summarized as follows,

- We introduce the free-energy theory for the NR-IQA task based on deep learning. To capture the image distortion, the pristine feature is estimated by the supervision of an FR-IQA model, mimicking the internal inference

This work is supported in part by the National Natural Science Foundation of China under 62022002, in part by Shenzhen Virtual University Park, The Science Technology and Innovation Committee of Shenzhen Municipality (Project No: 2021Szvup128), in part by the Hong Kong Research Grants Council General Research Fund (GRF) under Grant 11203220.

B. Chen, L. Zhu, C. Kong, H. Zhu and S. Wang are with the Department of Computer Science, City University of Hong Kong, Hong Kong (e-mail: blchen6-c@my.cityu.edu.hk; lingyuzhu-c@my.cityu.edu.hk; cqkong2-c@my.cityu.edu.hk; hwzhu4-c@my.cityu.edu.hk; shiqwang@cityu.edu.hk). Z. Li is with the Department of Computer Science and Electrical Engineering, University of Missouri-Kansas City, MO 64110, USA. (email:zhu.li@ieee.org). Corresponding author: Shiqi Wang.

mechanism in HVS.

- We learn the PR feature by a mutual learning strategy, leveraging the reference information. To improve the discrimination capability between the estimated PR feature and the distortion feature, a triplet loss is further adopted.
- We develop the aggregation strategy for the predicted scores of different patches in an image. The strategy benefits from the GRU, and generates the attention maps of the testing images for quality aggregation.

II. RELATED WORKS

Due to the lack of reference information, the existing NR-IQA measures can be classified into two categories: quality-aware feature extraction based NR-IQA and discrepancy estimation based NR-IQA. In the first category, the quality-aware features are extracted based on a natural scene statistics (NSS) model or a data-driven model, and the quality is finally predicted by a regression module. In the second category, the PR images are first constructed, then the discrepancy between the input images and its PR images is measured. The philosophy is that the larger the discrepancy, the worse quality the image possesses. Herein, we provide an overview of the two categories of NR-IQA models as well as the mutual learning methods.

A. Quality-Aware Feature Extraction based NR-IQA

Typically, conventional NR-IQA methods extract the quality-aware features based on the natural scene statistics (NSS) and predict the image quality by evaluating the destruction of naturalness. In [28], [29], based on the Mean-Subtracted Contrast-Normalized (MSCN) coefficients, the NSS are modeled with a generalized Gaussian distribution and the quality can be estimated by the distribution discrepancy. The NSS features have also been exploited in the wavelet domain, [12], [30]–[32]. In [31], to discriminate degraded and undegraded images, the complex pyramid wavelet transform is performed and the magnitudes and phases of the wavelet coefficients are characterized as the NSS descriptor. Analogously, in [11], the discrete cosine transform (DCT) is introduced for NSS model construction, leading to a Bayesian inference-based NR-IQA model. Considering the structural information is highly quality-relevant, the joint statistics of gradient magnitude and Laplacian of Gaussian response are utilized in [33] to model the statistical naturalness. In [34], the hybrid features consisting of texture components, structural information and intra-predicted modes are extracted and unified for adaptive bitrate estimation. Recently, there has been a surging interest in deep-feature extraction for NR-IQA. In [13], a shallow ConvNet is first utilized for patch-based NR-IQA learning. This work is extended by DeepBIQ [16], where a pre-trained convolutional neural network (CNN) is fine-tuned for the generic image description. Instead of learning only from the quality score, the multi-task CNN was proposed in [35], in which both the quality estimation and distortion identification are learned simultaneously for a better quality degradation measure. However, although those deep-learning based methods have achieved high-performance improvement,

insufficient training data usually create the over-fitting problem. To alleviate this issue, extra synthetic databases *e.g.* [36]–[38] have been proposed for more generalized model learning. The training data can also be enriched by ranking learning. In [38]–[41], the quality scores of an image pair are regressed and ranked, leading to the more quality-sensitive feature extraction. In [42], [43], to accelerate the model convergence, “Norm-in-Norm” loss was proposed. The embedded normalization has been proved to be able to improve the smoothness of the loss landscape. It is generally acknowledged that combining different databases for IQA can highly enrich the training samples. However, the annotation shift usually causes unreliable data fusion. In [44], Zhang *et al.* adopted rank-based learning to account for this problem, and the MOS uncertainty is also explored during optimization. The distortion type identification and quality regression are learned successively in [45], aiming to capture more accurate distortion.

B. Discrepancy Estimation based NR-IQA

The NR-IQA problem can be feasibly converted to the FR-IQA problem when the reference image can be inferred through generative models. In [46], the PR image is generated by a quality-aware generative network, then the discrepancy between the distorted image and PR image is measured for quality regression. In contrary to constructing the PR image with perfect quality, the reference information provided by the PR image that suffered from the severest distortion was explored in [47], then an NR-IQA metric was developed by measuring the similarity between the structures of distorted and the PR images. In [48], both a pristine reference image (generated via a restoration model) and a severely distorted image (generated via a degradation model) are utilized for quality prediction. Analogously, by comparing the distorted images and their two bidirectional PRs, the bilateral distance (error) maps are extracted in [49].

C. Mutual Learning

The assumption of mutual learning is highly relevant with the dual learning and collaborative learning, as their assumptions all lie in the encouragement of the models to teach each other during training. For example, the dual learning was adopted in [50], where two cross-lingual translation models are forced to learn from each other through the reinforcement learning. Comparing with dual learning, the same task is learned in the collaborative learning. In [51], multiple student models are expected to learn the same classification task while their inputs are sampled from different domains. Different from the dual learning and collaborative learning, both the tasks and inputs of the models in mutual learning are identical. For example, the deep mutual learning was utilized in [52], where two student models are forced to learn the classification collaboratively by a Kullback Leibler (KL) loss. This work was further extended in [53], with the KL loss replaced by a generative adversarial network. In our method, the mutual learning strategy was adopted to improve the learnability of the PR feature and we further impose the triplet constraint to the output features, significantly enhancing their discriminability.

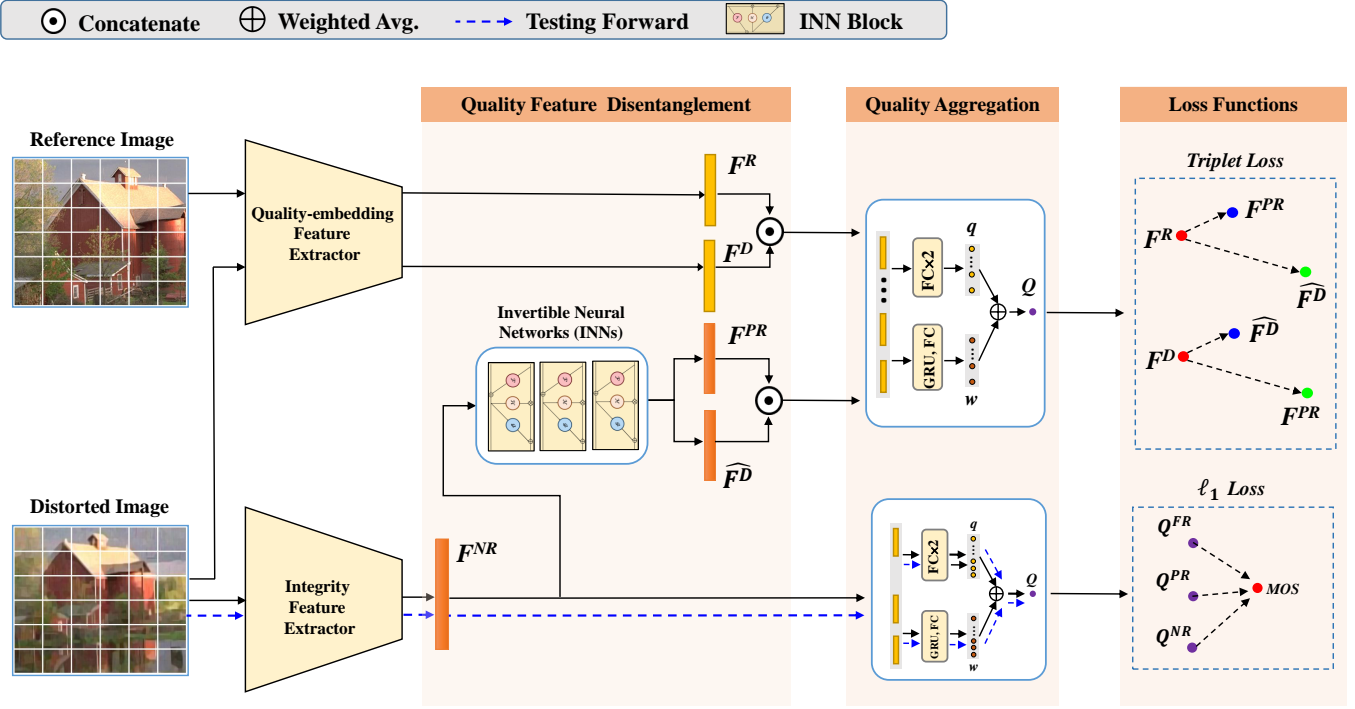


Fig. 1. Illustration of the framework of our proposed method. Two feature extractors are utilized in the training phase: the quality-embedding feature extractor and the integrity feature extractor. For the quality-embedding feature extractor, we extract the quality-embedding features F^D and F^R from the distortion image and its reference image, respectively. For the integrity feature extractor, we aim to extract the feature F^{NR} from a single distorted image that contains the fusion information of a PR feature F^{PR} and a distortion feature F^D by the guidance of F^R and F^D . Then the quality of the distorted image can be regressed by the F^{NR} . Finally, we propose a GRU-based quality aggregation module for patch-wise quality score aggregation. In the testing phase, only the testing image (without reference) is available for quality prediction based on the proposed NR-IQA model.

III. THE PROPOSED SCHEME

We aim to learn an NR-IQA measure by hallucinating the PR features. In the training stage, given the pristine reference, we attempt to build a FR-IQA model with the distorted and corresponding pristine reference images. The PR feature is subsequently learned in a mutual way. Finally, the GRU-based quality aggregation is performed to obtain the final quality score.

A. PR Feature Learning

As shown in Fig. 1, in the training phase, we learn to hallucinate the PR feature F^{PR} from a single distorted image by the guidance of the pristine reference feature F^R . In particular, the F^R is constructed from an FR model based on the quality-embedding feature extractor, and the F^{PR} is decomposed from the feature F^{NR} which is regarded as a fusion feature that contains the entire information of the PR feature F^{PR} and the distortion feature F^D .

In general, there are two properties a desired PR feature for quality prediction should possess. First, the PR feature should be learnable. Constructing the pristine image from the distorted one is usually a challenging task due to the corruption of content caused by different distortion types. For example, the texture regions could be difficult to be recovered when it is corrupted by blur distortion. Such challenges also bring the difficulties to learn pristine (PR) features. To account for this, self-supervised based methods can be adopted, such as the

generative adversarial network (GAN) based models [54], [55] or natural images prior based methods [56], [57]. As indicated in [58], the self-supervised learning methods greatly depend on the difficulty level of the task and the amount of training data. In this paper, we learn the PR feature in a supervised manner based on the reference as it is possible to obtain abundant pristine images. In particular, the features extracted from the reference images are used as guidance to provide a clear picture for the PR feature learning. Though in the training process the reference image could be taken advantage of, the PR feature may not be able to be feasibly learned by only forcing the inferred PR feature to be close to a pre-defined reference feature. As such, the learning capability of the NR-IQA network should be carefully considered during the reference feature estimation. In other words, when we learn the PR feature, the reference feature extraction should be learned mutually. Second, the PR feature should be discriminative enough when comparing with the distortion feature. Enhancing the discriminability could improve the quality sensitivity of the PR feature and subsequently promote the prediction performance.

The proposed method is conceptually appealing in the sense of learnability and discriminability. Regarding the learnability, a mutual learning strategy is adopted. As shown in Fig. 1, in the training process, the paired images including the distorted image and its corresponding reference are fed into the quality-embedding feature extractor, generating the reference feature F^R and distortion feature F^D . The integrity feature extractor,

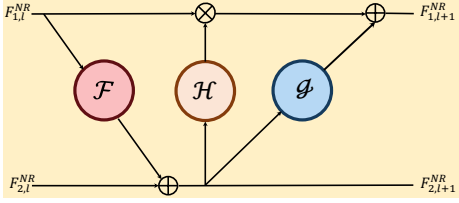


Fig. 2. The structure of invertible neural network.

which accepts the distorted image only, is encouraged to generate the feature F^{NR} with high quality-awareness. To this end, we force the F^{NR} to be derived from both the information of the pseudo reference feature F^{PR} and the distortion feature \hat{F}^D . As shown in Fig. 1, we adopt the invertible neural networks (INNs) [59], [60] to disentangle the F^{NR} into a pseudo reference feature F^{PR} and a distortion feature \hat{F}^D , without losing any information. Instead of using the concatenation of F^{PR} and \hat{F}^D for quality regression, the F^{NR} utilized enjoys higher quality awareness, generalization capability, and less inference time. In Fig. 2, we plot the structure of an INN block, which consists of transmission functions including \mathcal{F} , \mathcal{H} , and \mathcal{G} . For the l -th block, the F_l^{NR} is split into $F_{1,l}^{NR}$ and $F_{2,l}^{NR}$ along the channel axis, and they undergo the invertible transformations [59], [60] as follows,

$$\begin{aligned} F_{1,l+1}^{NR} &= F_{1,l}^{NR} + \mathcal{F}(F_{2,l}^{NR}), \\ F_{2,l+1}^{NR} &= F_{2,l}^{NR} \odot \exp(\mathcal{H}(F_{1,l+1}^{NR})) + \mathcal{G}(F_{1,l+1}^{NR}). \end{aligned} \quad (1)$$

The inverse transformation is computed as follows,

$$\begin{aligned} F_{2,l}^{NR} &= (F_{2,l+1}^{NR} - \mathcal{G}(F_{1,l+1}^{NR})) \odot \exp(-\mathcal{H}(F_{1,l+1}^{NR})) \\ F_{1,l}^{NR} &= F_{1,l+1}^{NR} - \mathcal{F}(F_{2,l}^{NR}). \end{aligned} \quad (2)$$

The outputs $F_{1,l+1}^{NR}$ and $F_{2,l+1}^{NR}$ are fed to the following INN blocks, and three blocks are finally utilized. We denote the output two features at the third block as F^{PR} and \hat{F}^D which are constrained by the triplet loss \mathcal{L}_{trip} for the discriminative reference feature learning.

The mutual learning strategy enables the integrity feature extractor and quality-embedding feature extractor to be learned simultaneously with the feature distance constraint. Thus, more learnable reference feature can be generated by the FR model. The connection among the features F^{NR} , F^{PR} and \hat{F}^D are constructed by an invertible layer, consisting of three invertible neural networks (INNs) [61]. Through the INNs, the integrity feature F^{NR} can be disentangled into a pseudo reference feature F^{PR} and a distortion feature \hat{F}^D , without losing any information due to the invertibility of INNs.

To equip the discriminative capability, a triplet loss is further utilized [62] as the distance measure between the reference features (F^R , F^{PR}) and the corresponding distortion features (F^D and \hat{F}^D), which is expressed as follows,

$$\begin{aligned} \mathcal{L}_{trip} &= \sum_{i=1}^N \left[\left\| F_i^R - F_i^{PR} \right\|_2^2 - \left\| F_i^R - \hat{F}_i^D \right\|_2^2 + \delta \right]_+ \\ &+ \sum_{i=1}^N \left[\left\| F_i^D - \hat{F}_i^D \right\|_2^2 - \left\| F_i^D - F_i^{PR} \right\|_2^2 + \delta \right]_+, \end{aligned} \quad (3)$$

where i is input patch index in a batch, N is the batch size and δ is a margin that is enforced between positive and negative pairs. With this loss, on the one hand, the distance between the reference feature and PR feature can be reduced. On the other hand, the discrepancies between the reference/PR feature and two distortion features can be enlarged.

As illustrated in Fig. 1, to maintain the relationship of F^{PR} and \hat{F}^D to be consistent with F^R and F^D , we concatenate F^R with F^D (denoted as $\text{Concat}(F^R, F^D)$) and F^{PR} with \hat{F}^D (denoted as $\text{Concat}(F^{PR}, \hat{F}^D)$) for quality prediction through a shared quality aggregation module.

B. GRU-Based Quality Aggregation

To aggregate the predicted quality score of each patch in an image, the aggregation module should be invariant of the patch numbers. In this paper, we propose a GRU-based quality score aggregation module as shown in Fig. 1. More specifically, regarding the concatenated features $\text{Concat}(F^R, F^D)$ and $\text{Concat}(F^{PR}, \hat{F}^D)$, two sub-branches are adopted for quality prediction. The first branch is a fully-connected (FC) layer that is responsible for patch-wise quality prediction with the patch-wise concatenated feature as input. Another sub-branch consists of one GRU layer and one FC layer. Different from [15], the inputs of the GRU layer are the features of all the patches in an image. With GRU, the long-term dependencies between different patches can be modeled and synthesized, then we normalize the output weights from the last FC layer for final attention map generation,

$$w_i = \frac{\alpha_i}{\sum_{j=1}^{N_p} \alpha_j}, \quad (4)$$

where i is the patch index in an image, and N_p is the number of patches. α_i and w_i are the predicted and normalized attention weights of i -th patch, respectively. Finally, the global image quality Q can be estimated as

$$Q = \sum_{i=1}^{N_p} w_i q_i = \frac{\sum_{i=1}^{N_p} \alpha_i q_i}{\sum_{i=1}^{N_p} \alpha_i}, \quad (5)$$

where q_i is the predicted quality of i -th patch. As shown in Fig. 1, we also adopt the same strategy (network) for the quality aggregation of the patch-wise integrity feature F^{NR} . Due to the distinct representations of the fused feature and concatenated features, the parameters of the two aggregation modules are not shared during the model training.

C. Objective Function

In summary, the objective function in our proposed method includes two triplet losses and three quality regression losses. In particular, for quality regression, compared with mean squared error (MSE), optimization with mean absolute error (MAE) is less sensitive to the outliers, leading to a more stable

training processing. Consequently, the objective function is given by,

$$\begin{aligned} \mathcal{L} &= \mathcal{L}_{mae} + \lambda \mathcal{L}_{trip} \\ &= \sum_{j=1}^{N_I} \left[\left| \hat{Q}_j - Q_j^{FR} \right| + \left| \hat{Q}_j - Q_j^{PR} \right| + \left| \hat{Q}_j - Q_j^{NR} \right| \right] \\ &\quad + \lambda \left(\sum_{i=1}^{N_I * N_P} \left[\left\| F_i^R - F_i^{PR} \right\|_2^2 - \left\| F_i^R - \hat{F}_i^D \right\|_2^2 + \delta \right]_+ \right) \\ &\quad + \lambda \left(\sum_{i=1}^{N_I * N_P} \left[\left\| F_i^D - \hat{F}_i^D \right\|_2^2 - \left\| F_i^D - F_i^{PR} \right\|_2^2 + \delta \right]_+ \right), \end{aligned} \quad (6)$$

where i and j are the patch index and image index, respectively. N_I is the number of images in a batch and \hat{Q}_j is the Mean Opinion Score (MOS) provided by the training set. Q^{FR} , Q^{PR} , Q^{NR} are the quality scores predicted from the features $Concat(F^R, F^D)$, $Concat(F^{PR}, \hat{F}^D)$ and F^{NR} , respectively. In addition, we adopt λ as the weight of the regularization term (\mathcal{L}_{trip}) for quality regression. It is also worth noting that the extractions of $F^R, F^D, F^{PR}, \hat{F}^D$ are not necessary in the testing phase, and we only adopt the Q^{NR} for the final quality prediction, thus the computational complexity in testing phase can be highly reduced comparing with the network used in the training phase.

IV. EXPERIMENTAL RESULTS

1) *IQA Databases*: Since our model is trained in a paired manner, the reference image should be available during the training phase. As such, to validate the proposed method, we evaluate our model on four synthetic natural databases including: TID2013 [25], LIVE [63], CSIQ [8] and KADID-10k [27]. More details are provided in Table I.

TID2013. The TID2013 database consists of 3,000 images obtained from 25 pristine images for reference. The pristine images are corrupted by 24 distortion types and each distortion type corresponds to 5 levels. The image quality is finally rated by double stimulus procedure and the MOS values are obtained in the range [0, 9], where larger MOS indicates better visual quality.

LIVE. The LIVE IQA database includes 982 distorted natural images and 29 reference images. Five different distortion types are included: JPEG and JPEG2000 compression, additive white Gaussian noise (WN), Gaussian blur (BLUR), and Rayleigh fast-fading channel distortion (FF). Different from the construction of TID2013, a single-stimulus rating procedure is adopted for quality rating, producing a range of different mean opinion scores (DMOS) from 0 to 100 and a lower DMOS value represents better image quality.

CSIQ. The CSIQ database contains 30 reference images and 866 distorted images. This database involves six distortion types: JPEG compression, JP2K compression, Gaussian blur, Gaussian white noise, Gaussian pink noise and contrast change. The images are rated by 35 different observers and the DMOS results are normalized into the range [0, 1].

KADID-10k. In this database, 81 pristine images are included and each pristine image is degraded by 25 distortion

types in 5 levels. All the images are resized into the same resolution (512×384). For each distorted image, 30 reliable degradation category ratings have been obtained by crowdsourcing.

2) *Implementation Details*: We implement our model by PyTorch [64]. In Fig. 3, we show the layer-wise network design of our proposed method. We crop the image patches without overlapping and the size is set by 64×64 . The number of image pairs in a batch is set by 32. We adopt Adam optimizer [65] for optimization. The learning rate is fixed to $1e-4$ with a weight decay set as $1e-4$. The weighting parameters λ, δ in Eqn. (6) are set as 20.0 and 0.5, respectively. We duplicate the samples by 16 times in a batch to augment the data. The maximum epoch is set by 1,000.

It should be mentioned that all the experimental pre-settings are fixed both in intra-database and cross-database training. For the intra-database evaluation, we randomly split the dataset into the training set, validation set and testing set by reference image to guarantee there is no content overlap among the three sets. In particular, 60%, 20%, 20% images are used for training, validation and testing, respectively. We discard the 25th reference image and the distorted versions in TID2013, as they are not natural image. The experimental results on intra-database are reported based on 10 random splits. To make errors and gradients comparable for different databases, we linearly map the MOS/DMOS ranges of the other three databases (TID2013, CSIQ, KADID-10k) to the DMOS range [0, 100] which is the same as LIVE database. Three evaluation metrics are reported for each experimental setting, including Spearman rank correlation coefficient (SRCC), Pearson linear correlation coefficient (PLCC) and perceptually weighted rank correlation (PWRC) [66]. The PLCC evaluates the prediction accuracy and the SRCC indicates the prediction monotonicity. Regarding the PWRC, the perceptual importance variation and subjective uncertainty are considered, which is confirmed to be reliable in recommending the perceptually preferred IQA model.

A. Quality Prediction on Intra-database

1) *Overall Performance on Individual Database*: In this sub-section, we compare our method with other state-of-the-art NR-IQA methods, including BRISQUE [28], M3 [33], FRIQUEE [67], CORNIA [68], DIIVIN [10], BLINDS-II [11], HOSA [69], Le-CNN [13], BIECON [14], WaDIQaM [15], ResNet-ft [70], IW-CNN [70], DB-CNN [70], CaHDC [71], HyperIQA [76] and Hallucinated-IQA [46]. The comparison results are shown in Tables II and III. All our experiments are conducted under ten times random train-test splitting operations, and the average SRCC and PLCC values are reported as final statistics. From the table, we can observe that all competing models achieve comparable performance on LIVE database while the performance vary on more challenging databases: TID2013 and KADID-10k. Comparing with hand-crafted based methods like BRISQUE, FRIQUEE and CORNIA, the CNN-based methods can achieve superior performance on different databases, revealing that human-perception relevant features can be learned from the training

TABLE I
DESCRIPTIONS OF THE FOUR IQA DATABASES.

Database	# of Ref. Images	# of Images	Distortion Types
TID2013 [25]	25	3,000	Additive Gaussian noise; Additive noise in color components; Spatially correlated noise; Masked noise; High frequency noise; Impulse noise; Quantization noise; Gaussian blur; Image denoising; JPEG compression; JPEG2000 compression; JPEG transmission errors; JPEG2000 transmission errors; Non eccentricity pattern noise; Local block-wise distortions of different intensity; Mean shift (intensity shift); Contrast change; Change of color saturation; Multiplicative Gaussian noise; Comfort noise; Lossy compression of noisy images; Image color quantization with dither; Chromatic aberrations; Sparse sampling and reconstruction
LIVE [63]	29	982	JPEG and JPEG2000 compression; Additive white; Gaussian noise; Gaussian blur; Rayleigh fast-fading channel distortion
CSIQ [8]	30	866	JPEG compression; JP2K compression; Gaussian blur; Gaussian white noise; Gaussian pink noise and contrast change
KADID-10k [27]	81	10,125	Blurs (Gaussian, lens,motion); Color related (diffusion, shifting, quantization, over-saturation and desaturation); Compression (JPEG2000, JPEG); Noise related (white, white with color, impulse, multiplicative white noise + denoise); Brightness changes (brighten, darken, shifting the mean); Spatial distortions (jitter, non-eccentricity patch, pixelate, quantization, color blocking); Sharpness and contrast.

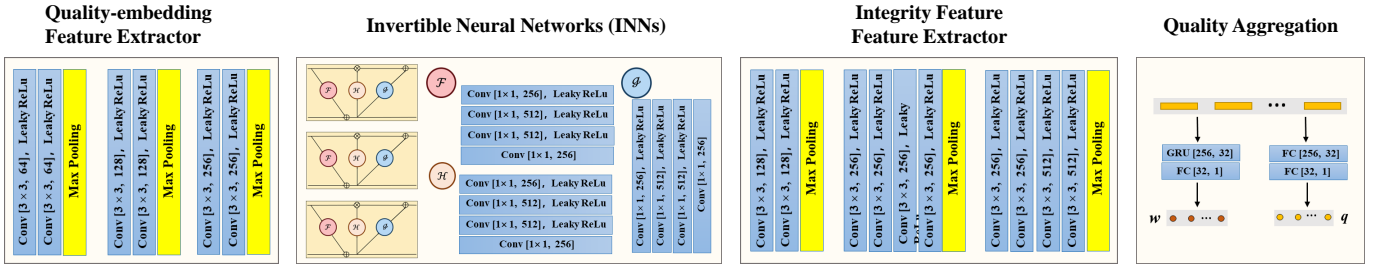


Fig. 3. Illustration of the network architectures for the quality-embedding feature extractor, INNs, integrity feature extractor and quality aggregation module.

TABLE II
PERFORMANCE EVALUATION ON THE LIVE, CSIQ AND TID2013 DATABASES. THE TOP TWO RESULTS ARE HIGHLIGHTED IN BOLDFACE.

Method	LIVE		CSIQ		TID2013	
	SRCC	PLCC	SRCC	PLCC	SRCC	PLCC
BRISQUE [28]	0.939	0.935	0.746	0.829	0.604	0.694
M3 [33]	0.951	0.950	0.795	0.839	0.689	0.771
FRIQUEE [67]	0.940	0.944	0.835	0.874	0.680	0.753
CORNIA [68]	0.947	0.950	0.678	0.776	0.678	0.768
HOSA [69]	0.946	0.947	0.741	0.823	0.735	0.815
Le-CNN [13]	0.956	0.953	-	-	-	-
BIECON [14]	0.961	0.962	0.815	0.823	0.717	0.762
DIQaM-NR [15]	0.960	0.972	-	-	0.835	0.855
WaDIQaM-NR [15]	0.954	0.963	-	-	0.761	0.787
ResNet-ft [70]	0.950	0.954	0.876	0.905	0.712	0.756
IW-CNN [70]	0.963	0.964	0.812	0.791	0.800	0.802
DB-CNN [70]	0.968	0.971	0.946	0.959	0.816	0.865
CaHDC [71]	0.965	0.964	0.903	0.914	0.862	0.878
HyperIQA [71]	0.962	0.966	0.923	0.942	0.729	0.775
Hallucinated-IQA [46]	0.982	0.982	0.885	0.910	0.879	0.880
FPR (Ours)	0.969	0.974	0.950	0.958	0.854	0.882
FPR (FR)	0.971	0.982	0.966	0.969	0.893	0.876

set. In particular, the PR image in Hallucinated-IQA is generated by a pixel-level generative network, leading to high demand for the number of training samples. This assumption can be verified by its poor performance on the CSIQ database. Moreover, we can also find that our method achieves the best performance on CSIQ and KADID-10k databases in terms of both SRCC and PLCC.

As we train our model in a paired manner, the FR results can also be acquired during the testing by involving the reference image. Herein, we also provide the FR results denoted as FPR (FR) in Tables II and III. From the tables, we can observe that our FR model can achieve higher performance when compared with our NR model, as the pristine image provide more accurate reference information for quality evaluation. We also observe that the performance of our FR model is not as good as some other FR models *e.g.*, WaDIQaM-FR [15]. We believe this is reasonable, as the learning capability of our NR model must be considered simultaneously during the extraction of reference feature. In Table IV, we further report the performance comparison in terms of PWRC. For a fair comparison, the same data splittings are performed for each method, and the average results of 10 repeated experiments

TABLE III
PERFORMANCE EVALUATION ON THE KADID-10K DATABASE. THE TOP TWO RESULTS ARE HIGHLIGHTED IN BOLDFACE.

Method	BIQI [30]	BLIINDS-II [11]	BRISQUE [28]	CORNIA [68]	DIIVINE [10]	HOSA [69]	SSEQ [72]
SROCC	0.431	0.527	0.519	0.541	0.489	0.609	0.424
PLCC	0.460	0.559	0.554	0.580	0.532	0.653	0.463
Method	InceptionResNetV2 [27]	WaDIQaM-NR [15]	DB-CNN [70]	HyperIQA [71]	LieartyIQA [42]	FPR (Ours)	FRP (FR)
SROCC	0.731	0.845	0.843	0.818	0.828	0.894	0.916
PLCC	0.734	0.851	0.845	0.818	0.818	0.898	0.911

TABLE IV
PWRC COMPARISON IN FOUR IQA DATABASES. THE TOP TWO RESULTS ARE HIGHLIGHTED IN BOLDFACE.

Method	CSIQ	KADID-10k	LIVE	TID2013
NIQE [73]	19.056	9.482	5.379	1.449
BRISQUE [28]	26.940	13.111	5.725	2.663
FRIQUEE [67]	25.515	22.454	5.860	4.031
ILNIQE [74]	25.695	14.989	5.216	2.640
DIQaM-NR [15]	25.528	17.941	4.915	3.019
WaDIQaM-NR [15]	27.221	25.205	5.770	4.547
DB-CNN [70]	29.312	21.805	5.810	4.634
HyperIQA [71]	26.388	22.214	5.471	4.386
LieartyIQA [42]	25.300	21.285	5.736	4.492
FPR (Ours)	30.328	25.492	5.920	5.515

are reported. From the Table IV, we can observe that our method achieves the best performance on each dataset. A significant performance gain can be acquired by our method on the TID2013 dataset, revealing our method is also effective for ranking image pairs with higher quality levels.

Furthermore, we compare our method with two PR image based NR-IQA methods named BPRI [47] and TSPR [49]. Following the experimental setting in [49] that four shared distortion types, *i.e.*, JPEG, GB, WN and JP2K in the TID2013, LIVE and CSIQ databases are used for performance comparison. The results are presented in Table V. We can observe that our method achieves the best performance in most settings and significantly outperforms the comparison methods in terms of the average SRCC values. These results reveal the effectiveness of our PR information constructed at the feature level. It also should be noted that compared with the generative adversarial networks (GAN) utilized in [46], [49] for reference information restoration at pixel-level, the lighter network in our method can significantly reduce the inference time.

2) *Performance on Individual Distortion Type*: To further explore the behaviors of our proposed method, we present the performance on individual distortion type and compare it with several competing NR-IQA models. The results of experiments performed on TID2013 database and LIVE database are shown in Table VI and Table VII, respectively. For each database, the average SRCC values of above ten settings are reported. As shown in the Table VI, we can easily observe that our method can achieve the highest accuracy on most distortion types (over 60% subsets). By contrast, lower SRCC values are obtained on some specific distortion types, *e.g.*, mean shift. The reason may lie in the challenge of PR feature hallucination due to

valuable information buried by the severe distortion. It is worth noting that our method achieves significant performance improvements on some noise-relevant distortion types (*e.g.*, additive Gaussian noise, masked noise) and compression-relevant distortion types (*e.g.*, JPEG compression, JPEG 2000 compression). The result is consistent with the performance on LIVE database, verifying the capacity that our model possesses in restoring the PR features from different distortion types.

B. Cross-Database Evaluation

To verify the generalization capability of our FPR model, we further evaluate our model on cross-database settings. We compare our method with seven NR-IQA methods, including: BRISQUE, M3, FRIQUEE, CORNIA, HOSA and two CNN-based counterparts DIQaM-NR and HyperIQA. The results of DIQaM-NR are reported from the original paper, and we re-train the HyperIQA by the source codes provided by the authors. All experiments are conducted with one database as training set and the other two databases as testing sets. We present the experimental results in VIII, from which we can find the model trained on LIVE (CSIQ) is easier to generalize to CSIQ (LIVE) as similar distortion types introduced by the two databases. However, it is a much more difficult task to generalize the model trained on CSIQ or LIVE to the TID2013 database, due to these unseen distortion types involved in TID2013 database. Despite this, we can still achieve a high SRCC in the two settings, demonstrating the superior generalization capability of our method.

C. Ablation Study

In this subsection, to reveal the functionalities of different modules in our proposed method, we perform the ablation study on TID2013 database. To be consistent with the experimental setting on intra-database, 60%, 20%, 20% images in TID2013 are grouped for training, validation and testing sets without content overlapping. Herein, we only report the ablation results by one fixed experimental splitting in Table IX. In particular, we first ablate the PR and INN modules from our model and retain the Integrity Feature Extractor and GRU-based Quality Aggregation modules. The performance drops dramatically due to the fact that no extra constraint be introduced to prevent the over-fitting problem. Then we replace the INN module by directly concatenating the learned pseudo reference feature and distortion feature for quality regression, resulting in the second ablation setting. The lower SRCC (0.86 *v.s.* 0.89) reveals that more generalized model can

TABLE V
SRCC COMPARISON IN THREE DATABASES ON FOUR COMMON DISTORTION TYPES. THE TOP TWO RESULTS ARE HIGHLIGHTED IN BOLDFACE.

Dataset	Dist.Type	Method										
		DIHVINE [10]	BLINDS-II [11]	BRISQUE [28]	CORNIA [68]	HOSA [69]	WaDIQaM-NR [15]	DIQA [75]	BPRI (c) [47]	BPRI (p) [47]	TSPR [49]	FPR (Ours)
LIVE	WN	0.988	0.947	0.979	0.976	0.975	0.970	0.988	0.984	0.985	0.972	0.987
	GB	0.923	0.915	0.951	0.969	0.954	0.960	0.962	0.927	0.924	0.978	0.979
	JPEG	0.921	0.950	0.965	0.955	0.954	0.964	0.976	0.967	0.967	0.947	0.932
	JP2K	0.922	0.930	0.914	0.943	0.954	0.949	0.961	0.908	0.907	0.950	0.965
CSIQ	WN	0.866	0.760	0.682	0.664	0.604	0.929	0.835	0.931	0.936	0.910	0.942
	GB	0.872	0.877	0.808	0.836	0.841	0.958	0.870	0.904	0.900	0.908	0.939
	JPEG	0.800	0.899	0.846	0.869	0.733	0.921	0.931	0.918	0.930	0.944	0.969
	JP2K	0.831	0.867	0.817	0.846	0.818	0.886	0.927	0.863	0.862	0.896	0.967
TID 2013	WN	0.855	0.647	0.858	0.817	0.817	0.843	0.915	0.918	0.918	0.876	0.931
	GB	0.834	0.837	0.814	0.840	0.870	0.861	0.912	0.873	0.859	0.837	0.912
	JPEG	0.628	0.836	0.845	0.896	0.986	0.931	0.875	0.907	0.910	0.913	0.906
	JP2K	0.853	0.888	0.893	0.901	0.902	0.932	0.912	0.883	0.868	0.935	0.900

TABLE VI
SRCC RESULTS OF INDIVIDUAL DISTORTION TYPES ON TID2013 DATABASE. THE TOP TWO RESULTS ARE HIGHLIGHTED IN BOLDFACE.

SRCC	BRISQUE [28]	M3 [33]	FRIQUEE [67]	CORNIA [68]	HOSA [69]	MEON [37]	DB-CNN [70]	FPR (Ours)
Additive Gaussian noise	0.711	0.766	0.730	0.692	0.833	0.813	0.790	0.953
Additive noise in color components	0.432	0.56	0.573	0.137	0.551	0.722	0.700	0.897
Spatially correlated noise	0.746	0.782	0.866	0.741	0.842	0.926	0.826	0.967
Masked noise	0.252	0.577	0.345	0.451	0.468	0.728	0.646	0.876
High frequency noise	0.842	0.900	0.847	0.815	0.897	0.911	0.879	0.934
Impulse noise	0.765	0.738	0.730	0.616	0.809	0.901	0.708	0.779
Quantization noise	0.662	0.832	0.764	0.661	0.815	0.888	0.825	0.920
Gaussian blur	0.871	0.896	0.881	0.850	0.883	0.887	0.859	0.833
Image denoising	0.612	0.709	0.839	0.764	0.854	0.797	0.865	0.944
JPEG compression	0.764	0.844	0.813	0.797	0.891	0.850	0.894	0.923
JPEG 2000 compression	0.745	0.885	0.831	0.846	0.919	0.891	0.916	0.923
JPEG transmission errors	0.301	0.375	0.498	0.694	0.73	0.746	0.772	0.797
JPEG 2000 transmission errors	0.748	0.718	0.660	0.686	0.710	0.716	0.773	0.752
Non-eccentricity pattern noise	0.269	0.173	0.076	0.200	0.242	0.116	0.270	0.559
Local block-wise distortions	0.207	0.379	0.032	0.027	0.268	0.500	0.444	0.265
Mean shift	0.219	0.119	0.254	0.232	0.211	0.177	-0.009	0.009
Contrast change	-0.001	0.155	0.585	0.254	0.362	0.252	0.548	0.699
Change of color saturation	0.003	-0.199	0.589	0.169	0.045	0.684	0.631	0.409
Multiplicative Gaussian noise	0.717	0.738	0.704	0.593	0.768	0.849	0.711	0.887
Comfort noise	0.196	0.353	0.318	0.617	0.622	0.406	0.752	0.830
Lossy compression of noisy images	0.609	0.692	0.641	0.712	0.838	0.772	0.860	0.982
Color quantization with dither	0.831	0.908	0.768	0.683	0.896	0.857	0.833	0.901
Chromatic aberrations	0.615	0.570	0.737	0.696	0.753	0.779	0.732	0.768
Sparse sampling and reconstruction	0.807	0.893	0.891	0.865	0.909	0.855	0.902	0.887

be learned by our INN module. As described before, the triplet loss \mathcal{L}_{trip} is adopted to learn more discriminative features. In this sense, we ablate the \mathcal{L}_{trip} in our third experiment. Again, a significant performance drop can be observed. The reason may lie in the quality discriminative feature learning resulting from the constraint of L_{trip} . Through L_{trip} , we build the PR feature F^{PR} and real one F^R by reducing their feature distance while enlarging the distance between the reference features (F^R , F^{PR}) and the corresponding distortion features (F^D and \hat{F}^D). Such constraints can force the model to exhaustively explore the feature difference caused by the distortion, and finally, the quality awareness and discrimination capability can be enhanced. Finally, three patch score aggregation modules are compared in Table IX. The superior performance further demonstrates the effectiveness of our GRU-based score aggregation module.

D. Feature Visualization

To better understand the performance of our proposed method, we visualize the quality relevant features F^R , F^{PR} ,

F^D and \hat{F}^D . More specifically, we first learn two models by our method on TID2013 database and LIVE database, respectively. Then 900 image pairs of each database are randomly sampled from the two databases for testing. For each database, we reduce the feature dimensions of F^R , F^{PR} , F^D and \hat{F}^D to three by T-SNE [78] and the results are visualized in Fig. 4. As shown in Fig. 4, we can observe that the discrepancy of the reference feature F^R and the pseudo reference feature F^{PR} is small due to the mutual learning strategy. By contrast, the large discrepancy can be acquired between the pseudo reference feature F^{PR} and distortion feature \hat{F}^D as the triplet loss performed, leading to the better performance.

In Fig. 5, we further visualize the feature maps of F^R , F^D , F^{PR} , \hat{F}^D and F^{NR} of several sampled distorted images. In particular, we reduce the channel dimension of F^D , F^R , \hat{F}^D , F^{PR} , and F^{NR} to 1 by average pooling for visualization. As shown in Fig. 5, we can observe that the distortion feature maps (F^D and \hat{F}^D) present a high activation on the distortion. For example, in the sub-figure (e), the local block distortion causes the high values at the distorted block regions in F^D

TABLE VII
AVERAGE SRCC AND PLCC RESULTS OF INDIVIDUAL DISTORTION TYPE ON LIVE DATABASE. THE TOP TWO RESULTS ARE HIGHLIGHTED IN BOLDFACE.

SRCC	JPEG	JP2K	WN	GB	FF
BRISQUE [28]	0.965	0.929	0.982	0.964	0.828
M3 [33]	0.966	0.930	0.986	0.935	0.902
FRIQUEE [67]	0.947	0.919	0.983	0.937	0.884
CORNIA [68]	0.947	0.924	0.958	0.951	0.921
HOSA [69]	0.954	0.935	0.975	0.954	0.954
dipIQ [77]	0.969	0.956	0.975	0.940	-
DB-CNN [70]	0.972	0.955	0.980	0.935	0.930
FPR (Ours)	0.962	0.960	0.986	0.959	0.966
PLCC	JPEG	JP2K	WN	GB	FF
BRISQUE [28]	0.971	0.940	0.989	0.965	0.894
M3 [33]	0.977	0.945	0.992	0.947	0.920
FRIQUEE [67]	0.955	0.935	0.991	0.949	0.936
CORNIA [68]	0.962	0.944	0.974	0.961	0.943
HOSA [69]	0.967	0.949	0.983	0.967	0.967
dipIQ [77]	0.980	0.964	0.983	0.948	-
DB-CNN [70]	0.986	0.967	0.988	0.956	0.961
FPR (Ours)	0.960	0.971	0.991	0.971	0.977

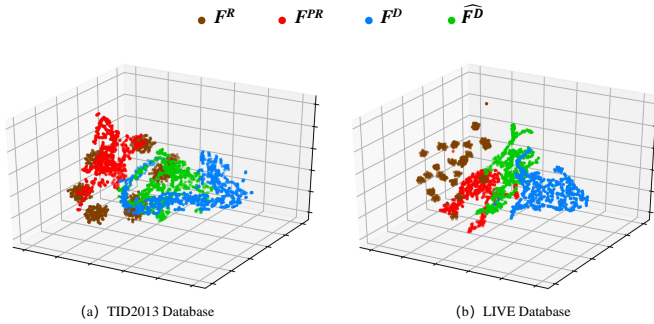


Fig. 4. T-SNE visualization of the features extracted from TID2013 and LIVE databases.

and \hat{F}^D . The inferred F^{PR} and \hat{F}^D are consistent with F^R and F^D even for different distortion types. Meanwhile, a significant difference can be observed between F^{PR} and \hat{F}^D due to the proposed triplet loss as a constraint.

E. Performance on Images from other Scenarios

The quality evaluation of images from other scenarios such as image enhancement datasets [79]–[83] and screen content image (SCI) datasets [84], [85] are also important tasks. To verify our model on those tasks, we further conduct experiments on one image enhancement dataset and two screen content image (SCI) datasets. In particular, the quality of the dehazing images is studied in the SHRQ dataset [82] and the quality of the distorted SCIs is studied in both SIQAD dataset [84] and SCID dataset [85]. Herein, we first provide a brief overview of the above datasets as follows,

- SHRQ dataset [82] consists of two subsets including the SHRQ-Regular and SHRQ-Aerial. The SHRQ-Regular includes 360 dehazed images created from 45 synthetic

hazy images while the SHRQ-Aerial includes 240 dehazed images created from 30 synthetic hazy images. In subjective testing, subjects need to rate the quality of the dehazed images using a five-grade continuous quality scale. Besides the dehazed image, the hazy image and the reference haze-free image are also provided.

- SIQAD dataset [84] contains 20 reference SCIs and 980 distorted SCIs. The distorted images are derived from seven distortion types including Gaussian Noise (GN), Gaussian Blur (GB), Motion Blur (MB), Contrast Change (CC), JPEG, JPEG2000, and Layer Segmentation based Coding (LSC). For each distortion type, seven distortion levels are generated.
- SCID dataset [85] consists of 1800 distorted SCIs generated by 40 reference images. In this dataset, nine distortion types are involved including GN, GB, MB, CC, JPEG compression, J2K, color saturation change (CSC), high-efficiency video coding screen content compression (HEVC-SCC), and Color quantization with dithering (CQD). Each distortion type contains five degradation levels. All the SCIs in SIQAD are with a resolution of 1280×720 .

We compare our method with the existing methods on those datasets and present the comparison results in Table X and Table XI. For the SHRQ dataset, our method achieves comparable performance with the latest method LiartyIQA [42]. For SCIs, our method is able to achieve the best performance on both the SIQAD dataset and SCID dataset, revealing the high generalization capability of our method on SCIs.

V. CONCLUSIONS

In this paper, we propose a novel NR-IQA method named FPR by restoring the reference information at feature-level. The image quality is evaluated by measuring the discrepancy at the feature-level and the PR feature is inferred based upon the INNs. The mutual learning strategy and triplet loss ensure the learnability and discriminability of PR features. To aggregate the patch-wise quality scores in an image, a GRU-based quality aggregation module is further proposed. The superior performance on the natural IQA databases, dehazing IQA databases, and screen content IQA databases demonstrates the effectiveness of our model. Moreover, our method also achieves promising performance on the cross-dataset settings, demonstrating the high generalization capability of our model.

REFERENCES

- [1] J. Guo and H. Chao, “Building an end-to-end spatial-temporal convolutional network for video super-resolution,” in *Proceedings of the AAAI Conference on Artificial Intelligence*, vol. 31, no. 1, 2017.
- [2] Y. Liu, J. Yan, and W. Ouyang, “Quality aware network for set to set recognition,” in *Proceedings of the IEEE Conference on Computer Vision and Pattern Recognition*, 2017, pp. 5790–5799.
- [3] K. Zhang, W. Zuo, S. Gu, and L. Zhang, “Learning deep cnn denoiser prior for image restoration,” in *Proceedings of the IEEE conference on computer vision and pattern recognition*, 2017, pp. 3929–3938.
- [4] J. Mannos and D. Sakrison, “The effects of a visual fidelity criterion of the encoding of images,” *IEEE transactions on Information Theory*, vol. 20, no. 4, pp. 525–536, 1974.
- [5] Z. Wang, A. C. Bovik, H. R. Sheikh, and E. P. Simoncelli, “Image quality assessment: from error visibility to structural similarity,” *IEEE transactions on image processing*, vol. 13, no. 4, pp. 600–612, 2004.

TABLE VIII
SRCC COMPARISON ON DIFFERENT CROSS-DATABASE SETTINGS. THE NUMBERS IN BOLD ARE THE BEST RESULTS.

Training	LIVE		CSIQ		TID2013	
Testing	CSIQ	TID2013	LIVE	TID2013	LIVE	CSIQ
BRISOUE [28]	0.562	0.358	0.847	0.454	0.790	0.590
M3 [33]	0.621	0.344	0.797	0.328	0.873	0.605
FRIQUEE [67]	0.722	0.461	0.879	0.463	0.755	0.635
CORNIA [68]	0.649	0.360	0.853	0.312	0.846	0.672
HOSA [69]	0.594	0.361	0.773	0.329	0.846	0.612
DIQaM-NR [15]	0.681	0.392	-	-	-	0.717
HyperIQA [71]	0.697	0.538	0.905	0.554	0.839	0.543
FPR (Ours)	0.620	0.433	0.895	0.522	0.884	0.732

TABLE IX
SRCC PERFORMANCE WITH ABLATION STUDIES PERFORMED ON THE TID2013 DATABASE.

Exp.ID	PR	INN	\mathcal{L}_{trip}	Patch Aggregation			SRCC
				Mean	Weighted	GRU	
1	✗	✗	✗			✓	0.670
2	✓	✗	✓			✓	0.859
3	✓	✓	✗			✓	0.772
4	✓	✓	✓	✓			0.869
5	✓	✓	✓		✓		0.848
6	✓	✓	✓			✓	0.887

TABLE X
PERFORMANCE COMPARISON ON THE DEHAZING DATASET SHRQ [82]. THE TOP TWO RESULTS ARE HIGHLIGHTED IN BOLDFACE.

Method	SHRQ-Aerial		SHRQ-Regular	
	SRCC	PLCC	SRCC	PLCC
NIQE [73]	0.401	0.579	0.414	0.579
BRISQUE [28]	0.370	0.510	0.414	0.744
FRIQUEE [67]	0.655	0.723	0.571	0.761
ILNIQE [74]	0.421	0.543	0.354	0.589
DIQaM-NR [15]	0.783	0.778	0.296	0.418
WaDIQaM-NR [15]	0.864	0.869	0.636	0.833
HyperIQA [71]	0.880	0.881	0.533	0.767
LieartyIQA [42]	0.914	0.921	0.720	0.880
FPR (Ours)	0.901	0.898	0.692	0.846

- [6] Z. Wang, E. P. Simoncelli, and A. C. Bovik, "Multiscale structural similarity for image quality assessment," in *The Thirty-Seventh Asilomar Conference on Signals, Systems & Computers, 2003*, vol. 2. Ieee, 2003, pp. 1398–1402.
- [7] L. Zhang, Y. Shen, and H. Li, "Vsi: A visual saliency-induced index for perceptual image quality assessment," *IEEE Transactions on Image processing*, vol. 23, no. 10, pp. 4270–4281, 2014.
- [8] E. C. Larson and D. M. Chandler, "Most apparent distortion: full-reference image quality assessment and the role of strategy," *Journal of electronic imaging*, vol. 19, no. 1, p. 011006, 2010.
- [9] H. R. Sheikh and A. C. Bovik, "Image information and visual quality," *IEEE Transactions on image processing*, vol. 15, no. 2, pp. 430–444, 2006.
- [10] A. K. Moorthy and A. C. Bovik, "Blind image quality assessment: From natural scene statistics to perceptual quality," *IEEE transactions on Image Processing*, vol. 20, no. 12, pp. 3350–3364, 2011.
- [11] M. A. Saad, A. C. Bovik, and C. Charrier, "Blind image quality assessment: A natural scene statistics approach in the dct domain," *IEEE transactions on Image Processing*, vol. 21, no. 8, pp. 3339–3352, 2012.
- [12] W. Hou, X. Gao, D. Tao, and X. Li, "Blind image quality assessment via deep learning," *IEEE transactions on neural networks and learning systems*, vol. 26, no. 6, pp. 1275–1286, 2014.
- [13] L. Kang, P. Ye, Y. Li, and D. Doermann, "Convolutional neural networks for no-reference image quality assessment," in *Proceedings of the IEEE conference on computer vision and pattern recognition*, 2014, pp. 1733–1740.
- [14] J. Kim and S. Lee, "Fully deep blind image quality predictor," *IEEE Journal of selected topics in signal processing*, vol. 11, no. 1, pp. 206–220, 2016.
- [15] S. Bosse, D. Maniry, K.-R. Müller, T. Wiegand, and W. Samek, "Deep neural networks for no-reference and full-reference image quality assessment," *IEEE Transactions on image processing*, vol. 27, no. 1, pp.

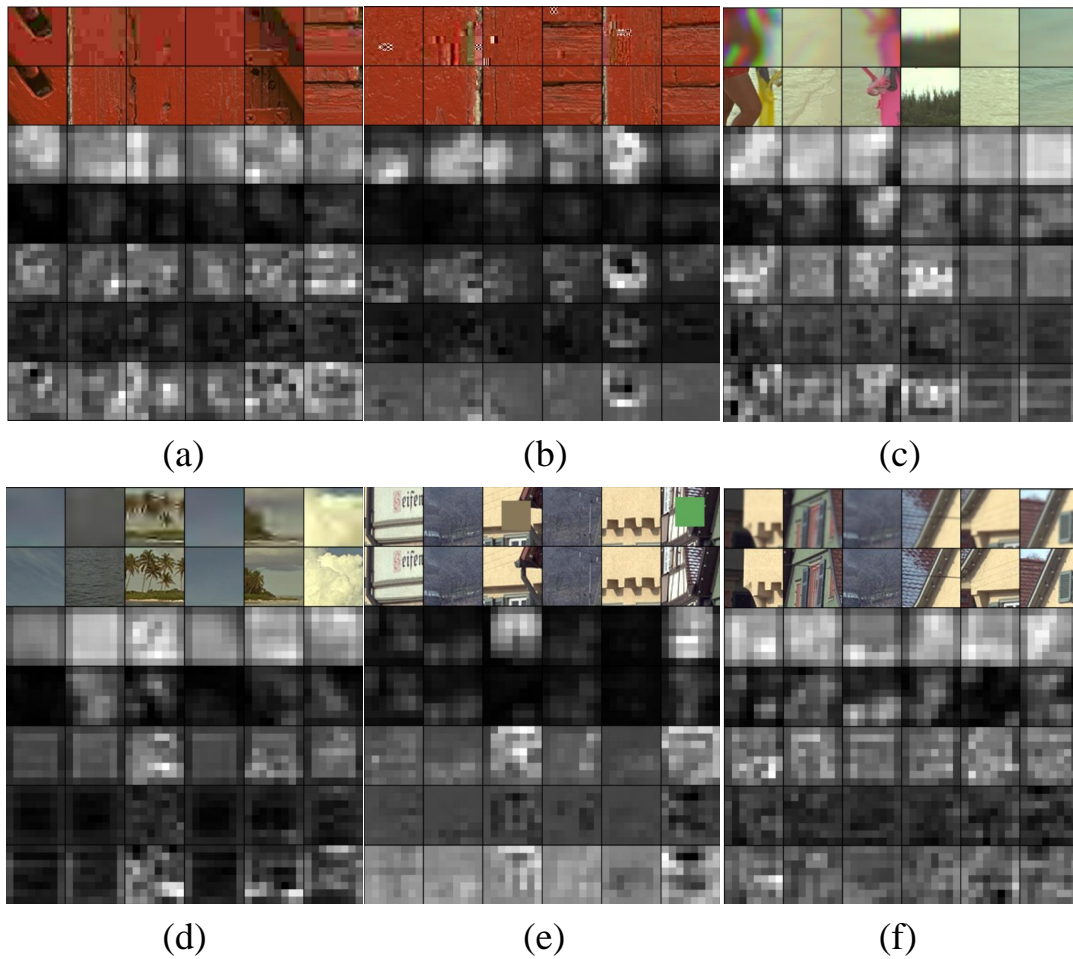


Fig. 5. Visualizations of the extracted feature maps. In each sub-figure, from up to down, are the sampled distorted image patches I^R , the reference image patches I^D , the corresponding F^D , F^R , \hat{F}^D , F^{FPR} and F^{FNR} are presented, respectively. The images are distorted by: (a) JPEG compression, (b) JPEG transmission errors, (c) Chromatic aberrations, (d) JPEG2000 compression, (e) Local block-wise distortions of different intensity, and (f) Gaussian blur.

- 206–219, 2017.
- [16] S. Bianco, L. Celona, P. Napoletano, and R. Schettini, “On the use of deep learning for blind image quality assessment,” *Signal, Image and Video Processing*, vol. 12, no. 2, pp. 355–362, 2018.
- [17] J. Gu, G. Meng, S. Xiang, and C. Pan, “Blind image quality assessment via learnable attention-based pooling,” *Pattern Recognition*, vol. 91, pp. 332–344, 2019.
- [18] J. Fu, H. Wang, and L. Zuo, “Blind image quality assessment for multiply distorted images via convolutional neural networks,” in *2016 IEEE International Conference on Acoustics, Speech and Signal Processing (ICASSP)*. IEEE, 2016, pp. 1075–1079.
- [19] J. Kim, A.-D. Nguyen, S. Ahn, C. Luo, and S. Lee, “Multiple level feature-based universal blind image quality assessment model,” in *2018 25th IEEE International Conference on Image Processing (ICIP)*. IEEE, 2018, pp. 291–295.
- [20] K. Friston, J. Kilner, and L. Harrison, “A free energy principle for the brain,” *Journal of Physiology-Paris*, vol. 100, no. 1-3, pp. 70–87, 2006.
- [21] K. Friston, “The free-energy principle: a unified brain theory?” *Nature reviews neuroscience*, vol. 11, no. 2, pp. 127–138, 2010.
- [22] K. Gu, G. Zhai, X. Yang, and W. Zhang, “Using free energy principle for blind image quality assessment,” *IEEE Transactions on Multimedia*, vol. 17, no. 1, pp. 50–63, 2014.
- [23] G. Zhai, X. Wu, X. Yang, W. Lin, and W. Zhang, “A psychovisual quality metric in free-energy principle,” *IEEE Transactions on Image Processing*, vol. 21, no. 1, pp. 41–52, 2011.
- [24] J. Chung, C. Gulcehre, K. Cho, and Y. Bengio, “Empirical evaluation of gated recurrent neural networks on sequence modeling,” *arXiv preprint arXiv:1412.3555*, 2014.
- [25] N. Ponomarenko, L. Jin, O. Ieremeiev, V. Lukin, K. Egiazarian, J. Astola, B. Vozel, K. Chehdi, M. Carli, F. Battisti *et al.*, “Image database tid2013: Peculiarities, results and perspectives,” *Signal Processing: Image Communication*, vol. 30, pp. 57–77, 2015.
- [26] H. R. Sheikh, M. F. Sabir, and A. C. Bovik, “A statistical evaluation of recent full reference image quality assessment algorithms,” *IEEE Transactions on image processing*, vol. 15, no. 11, pp. 3440–3451, 2006.
- [27] H. Lin, V. Hosu, and D. Saupe, “Kadid-10k: A large-scale artificially distorted iqa database,” in *2019 Eleventh International Conference on Quality of Multimedia Experience (QoMEX)*, 2019.
- [28] A. Mittal, A. K. Moorthy, and A. C. Bovik, “No-reference image quality assessment in the spatial domain,” *IEEE Transactions on image processing*, vol. 21, no. 12, pp. 4695–4708, 2012.
- [29] P. Ye, J. Kumar, L. Kang, and D. Doermann, “Real-time no-reference image quality assessment based on filter learning,” in *Proceedings of the IEEE Conference on Computer Vision and Pattern Recognition*, 2013, pp. 987–994.
- [30] A. K. Moorthy and A. C. Bovik, “A two-step framework for constructing blind image quality indices,” *IEEE Signal processing letters*, vol. 17, no. 5, pp. 513–516, 2010.
- [31] H. Tang, N. Joshi, and A. Kapoor, “Learning a blind measure of perceptual image quality,” in *CVPR 2011*. IEEE, 2011, pp. 305–312.
- [32] Z. Wang, G. Wu, H. R. Sheikh, E. P. Simoncelli, E.-H. Yang, and A. C. Bovik, “Quality-aware images,” *IEEE transactions on image processing*, vol. 15, no. 6, pp. 1680–1689, 2006.
- [33] W. Xue, X. Mou, L. Zhang, A. C. Bovik, and X. Feng, “Blind image quality assessment using joint statistics of gradient magnitude and laplacian features,” *IEEE Transactions on Image Processing*, vol. 23, no. 11, pp. 4850–4862, 2014.
- [34] Y. Sun, L. Li, Z. Li, and S. Liu, “Referenceless rate-distortion modeling

TABLE XI
PERFORMANCE COMPARISON ON SIQAD [84] AND SCID [85] DATASETS. THE TOP TWO RESULTS ARE HIGHLIGHTED IN BOLDFACE.

SIQAD									
Method	NIQE [73]	IL-NIQE [74]	BRISQUE [28]	DIIVINE [10]	QAC [86]	CORNIA [68]	HOSA [69]	BQMS [87]	SIQE [88]
SRCC	0.359	0.320	0.775	0.659	0.301	0.788	0.718	0.725	0.763
PLCC	0.381	0.386	0.811	0.691	0.375	0.815	0.766	0.758	0.791
Method	ASIQE [88]	CLGF [89]	NRLT [90]	DIQA-NR [15]	WaDIQA-NR [15]	HRFF [91]	Yang <i>et al.</i> (TIP21) [92]	Yang <i>et al.</i> (Tcy20) [93]	FPR (Ours)
SRCC	0.757	0.811	0.822	0.860	0.862	0.832	0.834	0.854	0.873
PLCC	0.788	0.833	0.844	0.871	0.877	0.852	0.853	0.874	0.886
SCID									
Method	NIQE [73]	IL-NIQE [74]	BRISQUE [28]	DIIVINE [10]	QAC [86]	CORNIA [68]	HOSA [69]	BQMS [87]	SIQE [88]
SRCC	0.280	0.102	0.471	0.436	0.557	0.672	0.690	0.613	0.601
PLCC	0.322	0.260	0.520	0.462	0.585	0.694	0.711	0.619	0.634
Method	ASIQE [88]	CLGF [89]	NRLT [90]	DIQA-NR [15]	WaDIQA-NR [15]	HRFF [91]	Yang <i>et al.</i> (TIP21) [92]	Yang <i>et al.</i> (Tcy20) [93]	FPR (Ours)
SRCC	0.605	0.687	0.609	0.721	0.758	-	0.692	0.756	0.852
PLCC	0.638	0.698	0.622	0.740	0.766	-	0.715	0.787	0.856

- with learning from bitstream and pixel features,” in *MM '20: The 28th ACM International Conference on Multimedia, Virtual Event / Seattle, WA, USA, October 12-16, 2020*. ACM, 2020, pp. 2481–2489. [Online]. Available: <https://doi.org/10.1145/3394171.3413545>
- [35] L. Kang, P. Ye, Y. Li, and D. Doermann, “Simultaneous estimation of image quality and distortion via multi-task convolutional neural networks,” in *2015 IEEE international conference on image processing (ICIP)*. IEEE, 2015, pp. 2791–2795.
- [36] W. Zhang, K. Ma, J. Yan, D. Deng, and Z. Wang, “Blind image quality assessment using a deep bilinear convolutional neural network,” *IEEE Transactions on Circuits and Systems for Video Technology*, 2018.
- [37] K. Ma, W. Liu, K. Zhang, Z. Duanmu, Z. Wang, and W. Zuo, “End-to-end blind image quality assessment using deep neural networks,” *IEEE Transactions on Image Processing*, vol. 27, no. 3, pp. 1202–1213, 2017.
- [38] B. Chen, H. Li, H. Fan, and S. Wang, “No-reference screen content image quality assessment with unsupervised domain adaptation,” *IEEE Transactions on Image Processing*, 2021.
- [39] X. Liu, J. van de Weijer, and A. D. Bagdanov, “Rankiq: Learning from rankings for no-reference image quality assessment,” in *Proceedings of the IEEE International Conference on Computer Vision*, 2017, pp. 1040–1049.
- [40] Y. Niu, D. Huang, Y. Shi, and X. Ke, “Siamese-network-based learning to rank for no-reference 2d and 3d image quality assessment,” *IEEE Access*, vol. 7, pp. 101 583–101 595, 2019.
- [41] Z. Ying, D. Pan, and P. Shi, “Quality difference ranking model for smartphone camera photo quality assessment,” in *2020 IEEE International Conference on Multimedia & Expo Workshops (ICMEW)*. IEEE, 2020, pp. 1–6.
- [42] D. Li, T. Jiang, and M. Jiang, “Norm-in-norm loss with faster convergence and better performance for image quality assessment,” in *Proceedings of the 28th ACM International Conference on Multimedia*, 2020, pp. 789–797.
- [43] —, “Unified quality assessment of in-the-wild videos with mixed datasets training,” *International Journal of Computer Vision*, vol. 129, no. 4, pp. 1238–1257, 2021.
- [44] W. Zhang, K. Ma, G. Zhai, and X. Yang, “Uncertainty-aware blind image quality assessment in the laboratory and wild,” *IEEE Transactions on Image Processing*, vol. 30, pp. 3474–3486, 2021.
- [45] C. Yan, T. Teng, Y. Liu, Y. Zhang, H. Wang, and X. Ji, “Precise no-reference image quality evaluation based on distortion identification,” *ACM Transactions on Multimedia Computing, Communications, and Applications (TOMM)*, vol. 17, no. 3s, pp. 1–21, 2021.
- [46] K.-Y. Lin and G. Wang, “Hallucinated-iqa: No-reference image quality assessment via adversarial learning,” in *Proceedings of the IEEE Conference on Computer Vision and Pattern Recognition*, 2018, pp. 732–741.
- [47] X. Min, K. Gu, G. Zhai, J. Liu, X. Yang, and C. W. Chen, “Blind quality assessment based on pseudo-reference image,” *IEEE Transactions on Multimedia*, vol. 20, no. 8, pp. 2049–2062, 2017.
- [48] Q. Jiang, Z. Peng, G. Yue, H. Li, and F. Shao, “No-reference image contrast evaluation by generating bi-directional pseudo references,” *IEEE Transactions on Industrial Informatics*, 2020.
- [49] J. Hu, X. Wang, F. Shao, and Q. Jiang, “Tspr: Deep network-based blind image quality assessment using two-side pseudo reference images,” *Digital Signal Processing*, vol. 106, p. 102849, 2020.
- [50] D. He, Y. Xia, T. Qin, L. Wang, N. Yu, T.-Y. Liu, and W.-Y. Ma, “Dual learning for machine translation,” *Advances in neural information processing systems*, vol. 29, pp. 820–828, 2016.
- [51] T. Batra and D. Parikh, “Cooperative learning with visual attributes,” *arXiv preprint arXiv:1705.05512*, 2017.
- [52] Y. Zhang, T. Xiang, T. M. Hospedales, and H. Lu, “Deep mutual learning,” in *Proceedings of the IEEE Conference on Computer Vision and Pattern Recognition*, 2018, pp. 4320–4328.
- [53] X. Lai and Y. Qu, “Adversarial deep mutual learning,” in *2019 IEEE International Conference on Unmanned Systems and Artificial Intelligence (ICUSAI)*. IEEE, 2019, pp. 324–329.
- [54] H.-U. Kim, Y. J. Koh, and C.-S. Kim, “Global and local enhancement networks for paired and unpaired image enhancement,” in *European Conference on Computer Vision*. Springer, 2020, pp. 339–354.
- [55] Y.-S. Chen, Y.-C. Wang, M.-H. Kao, and Y.-Y. Chuang, “Deep photo enhancer: Unpaired learning for image enhancement from photographs with gans,” in *Proceedings of the IEEE Conference on Computer Vision and Pattern Recognition*, 2018, pp. 6306–6314.
- [56] M. Noroozi and P. Favaro, “Unsupervised learning of visual representations by solving jigsaw puzzles,” in *European conference on computer vision*. Springer, 2016, pp. 69–84.
- [57] Y. Zhang, X. Di, B. Zhang, Q. Li, S. Yan, and C. Wang, “Self-supervised low light image enhancement and denoising,” *arXiv preprint arXiv:2103.00832*, 2021.
- [58] L. Jing and Y. Tian, “Self-supervised visual feature learning with deep neural networks: A survey,” *IEEE transactions on pattern analysis and machine intelligence*, vol. 43, no. 11, pp. 4037–4058, 2020.
- [59] L. Dinh, D. Krueger, and Y. Bengio, “Nice: Non-linear independent components estimation,” *arXiv preprint arXiv:1410.8516*, 2014.
- [60] L. Dinh, J. Sohl-Dickstein, and S. Bengio, “Density estimation using real nvp,” *arXiv preprint arXiv:1605.08803*, 2016.
- [61] L. Ardizzone, J. Kruse, S. Wirkert, D. Rahner, E. W. Pellegrini, R. S. Klessen, L. Maier-Hein, C. Rother, and U. Köthe, “Analyzing inverse problems with invertible neural networks,” *arXiv preprint arXiv:1808.04730*, 2018.
- [62] F. Schroff, D. Kalenichenko, and J. Philbin, “Facenet: A unified embedding for face recognition and clustering,” in *Proceedings of the IEEE conference on computer vision and pattern recognition*, 2015, pp. 815–823.
- [63] H. R. Sheikh, “Image and video quality assessment research at live,” <http://live.ece.utexas.edu/research/quality>, 2003.
- [64] A. Paszke, S. Gross, F. Massa, A. Lerer, J. Bradbury, G. Chanan, T. Killeen, Z. Lin, N. Gimelshein, L. Antiga *et al.*, “Pytorch: An imperative style, high-performance deep learning library,” in *Advances in neural information processing systems*, 2019, pp. 8026–8037.
- [65] D. P. Kingma and J. Ba, “Adam: A method for stochastic optimization,” *arXiv preprint arXiv:1412.6980*, 2014.
- [66] Q. Wu, H. Li, F. Meng, and K. N. Ngan, “A perceptually weighted rank correlation indicator for objective image quality assessment,” *IEEE Transactions on Image Processing*, vol. 27, no. 5, pp. 2499–2513, 2018.

- [67] D. Ghadiyaram and A. C. Bovik, "Perceptual quality prediction on authentically distorted images using a bag of features approach," *Journal of vision*, vol. 17, no. 1, pp. 32–32, 2017.
- [68] P. Ye, J. Kumar, L. Kang, and D. Doermann, "Unsupervised feature learning framework for no-reference image quality assessment," in *2012 IEEE conference on computer vision and pattern recognition*. IEEE, 2012, pp. 1098–1105.
- [69] J. Xu, P. Ye, Q. Li, H. Du, Y. Liu, and D. Doermann, "Blind image quality assessment based on high order statistics aggregation," *IEEE Transactions on Image Processing*, vol. 25, no. 9, pp. 4444–4457, 2016.
- [70] J. Kim and S. Lee, "Deep learning of human visual sensitivity in image quality assessment framework," in *Proceedings of the IEEE conference on computer vision and pattern recognition*, 2017, pp. 1676–1684.
- [71] J. Wu, J. Ma, F. Liang, W. Dong, G. Shi, and W. Lin, "End-to-end blind image quality prediction with cascaded deep neural network," *IEEE Transactions on Image Processing*, vol. 29, pp. 7414–7426, 2020.
- [72] L. Liu, B. Liu, H. Huang, and A. C. Bovik, "No-reference image quality assessment based on spatial and spectral entropies," *Signal Processing: Image Communication*, vol. 29, no. 8, pp. 856–863, 2014.
- [73] A. Mittal, R. Soundararajan, and A. C. Bovik, "Making a "completely blind" image quality analyzer," *IEEE Signal processing letters*, vol. 20, no. 3, pp. 209–212, 2012.
- [74] L. Zhang, L. Zhang, and A. C. Bovik, "A feature-enriched completely blind image quality evaluator," *IEEE Transactions on Image Processing*, vol. 24, no. 8, pp. 2579–2591, 2015.
- [75] J. Kim, A.-D. Nguyen, and S. Lee, "Deep cnn-based blind image quality predictor," *IEEE transactions on neural networks and learning systems*, vol. 30, no. 1, pp. 11–24, 2018.
- [76] S. Su, Q. Yan, Y. Zhu, C. Zhang, X. Ge, J. Sun, and Y. Zhang, "Blindly assess image quality in the wild guided by a self-adaptive hyper network," in *Proceedings of the IEEE/CVF Conference on Computer Vision and Pattern Recognition*, 2020, pp. 3667–3676.
- [77] K. Ma, W. Liu, T. Liu, Z. Wang, and D. Tao, "dipiqa: Blind image quality assessment by learning-to-rank discriminable image pairs," *IEEE Transactions on Image Processing*, vol. 26, no. 8, pp. 3951–3964, 2017.
- [78] L. v. d. Maaten and G. Hinton, "Visualizing data using t-sne," *Journal of machine learning research*, vol. 9, no. Nov, pp. 2579–2605, 2008.
- [79] Q. Wu, L. Wang, K. N. Ngan, H. Li, and F. Meng, "Beyond synthetic data: A blind deraining quality assessment metric towards authentic rain image," in *2019 IEEE International Conference on Image Processing (ICIP)*. IEEE, 2019, pp. 2364–2368.
- [80] Q. Wu, L. Wang, K. N. Ngan, H. Li, F. Meng, and L. Xu, "Subjective and objective de-raining quality assessment towards authentic rain image," *IEEE Transactions on Circuits and Systems for Video Technology*, vol. 30, no. 11, pp. 3883–3897, 2020.
- [81] Q. Wu, H. Li, F. Meng, and K. N. Ngan, "Q-dnn: A quality-aware deep neural network for blind assessment of enhanced images," in *2016 Visual Communications and Image Processing (VCIP)*. IEEE, 2016, pp. 1–4.
- [82] X. Min, G. Zhai, K. Gu, Y. Zhu, J. Zhou, G. Guo, X. Yang, X. Guan, and W. Zhang, "Quality evaluation of image dehazing methods using synthetic hazy images," *IEEE Transactions on Multimedia*, vol. 21, no. 9, pp. 2319–2333, 2019.
- [83] L. Wang, Q. Wu, K. N. Ngan, H. Li, F. Meng, and L. Xu, "Blind tone-mapped image quality assessment and enhancement via disentangled representation learning," in *2020 Asia-Pacific Signal and Information Processing Association Annual Summit and Conference (APSIPA ASC)*. IEEE, 2020, pp. 1096–1102.
- [84] H. Yang, Y. Fang, and W. Lin, "Perceptual quality assessment of screen content images," *IEEE Transactions on Image Processing*, vol. 24, no. 11, pp. 4408–4421, 2015.
- [85] Z. Ni, L. Ma, H. Zeng, Y. Fu, L. Xing, and K.-K. Ma, "Scid: A database for screen content images quality assessment," in *2017 International Symposium on Intelligent Signal Processing and Communication Systems (ISPACS)*. IEEE, 2017, pp. 774–779.
- [86] W. Xue, L. Zhang, and X. Mou, "Learning without human scores for blind image quality assessment," in *Proceedings of the IEEE conference on computer vision and pattern recognition*, 2013, pp. 995–1002.
- [87] K. Gu, G. Zhai, W. Lin, X. Yang, and W. Zhang, "Learning a blind quality evaluation engine of screen content images," *Neurocomputing*, vol. 196, pp. 140–149, 2016.
- [88] K. Gu, J. Zhou, J.-F. Qiao, G. Zhai, W. Lin, and A. C. Bovik, "No-reference quality assessment of screen content pictures," *IEEE Transactions on Image Processing*, vol. 26, no. 8, pp. 4005–4018, 2017.
- [89] J. Wu, Z. Xia, H. Zhang, and H. Li, "Blind quality assessment for screen content images by combining local and global features," *Digital Signal Processing*, vol. 91, pp. 31–40, 2019.
- [90] Y. Fang, J. Yan, L. Li, J. Wu, and W. Lin, "No reference quality assessment for screen content images with both local and global feature representation," *IEEE Transactions on Image Processing*, vol. 27, no. 4, pp. 1600–1610, 2017.
- [91] L. Zheng, L. Shen, J. Chen, P. An, and J. Luo, "No-reference quality assessment for screen content images based on hybrid region features fusion," *IEEE Transactions on Multimedia*, vol. 21, no. 8, pp. 2057–2070, 2019.
- [92] J. Yang, Z. Bian, J. Liu, B. Jiang, W. Lu, X. Gao, and H. Song, "No-reference quality assessment for screen content images using visual edge model and adaboosting neural network," *IEEE Transactions on Image Processing*, vol. 30, pp. 6801–6814, 2021.
- [93] J. Yang, Y. Zhao, J. Liu, B. Jiang, Q. Meng, W. Lu, and X. Gao, "No reference quality assessment for screen content images using stacked autoencoders in pictorial and textual regions," *IEEE transactions on cybernetics*, 2020.



learning.

Baoliang Chen received his B.S. degree in Electronic Information Science and Technology from Hefei University of Technology, Hefei, China, in 2015, his M.S. degree in Intelligent Information Processing from Xidian University, Xian, China, in 2018, and his Ph.D. degree in computer science from the City University of Hong Kong, Hong Kong, in 2022. He is currently a postdoctoral researcher with the Department of Computer Science, City University of Hong Kong. His research interests include image/video quality assessment and transfer



Lingyu Zhu received the B.S. degree from the Wuhan University of Technology in 2018 and the master's degree from Hong Kong University of Science and Technology in 2019. He is currently pursuing a Ph.D. degree at the City University of Hong Kong. His research interests include image/video quality assessments, image/ video processing, and deep learning.



Chenqi Kong received the B.S. and M.S. degrees in Harbin Institute of Technology, Harbin, China, in 2017 and 2019, respectively. He is currently pursuing a Ph.D. degree in the Department of Computer Science, City University of Hong Kong, Hong Kong, China (Hong Kong SAR). His research interests include computer vision and multimedia forensics.



Hanwei Zhu received the B.E and M.S. degrees from the Jiangxi University of Finance and Economics, Nanchang, China, in 2017 and 2020, respectively. He is currently pursuing a Ph.D. degree in the Department of Computer Science, City University of Hong Kong. His research interest includes perceptual image processing and computational photography.



Shiqi Wang (Senior Member, IEEE) received the B.S. degree in computer science from the Harbin Institute of Technology in 2008 and the Ph.D. degree in computer application technology from Peking University in 2014. From 2014 to 2016, he was a Post-Doctoral Fellow with the Department of Electrical and Computer Engineering, University of Waterloo, Waterloo, ON, Canada. From 2016 to 2017, he was a Research Fellow with the Rapid-Rich Object Search Laboratory, Nanyang Technological University, Singapore. He is currently an Assistant

Professor with the Department of Computer Science, City University of Hong Kong. He has proposed over 40 technical proposals to ISO/MPEG, ITU-T, and AVS standards, and authored/coauthored more than 200 refereed journal articles/conference papers. He received the Best Paper Award from IEEE VCIP 2019, ICME 2019, IEEE Multimedia 2018, and PCM 2017 and is the coauthor of an article that received the Best Student Paper Award in the IEEE ICIP 2018. His research interests include video compression, image/video quality assessment, and image/video search and analysis.



Zhu Li (Senior Member, IEEE) is a professor with the Dept of Computer Science & Electrical Engineering (CSEE), University of Missouri, Kansas City, and director of the NSF I/UCRC Center for Big Learning (CBL) at UMKC. He received his Ph.D. in Electrical & Computer Engineering from Northwestern University, Evanston in 2004. He was AFOSR SFFP summer faculty at the US Air Force Academy (USAFA), 2016-18, 2020, and 2022. He was Sr. Staff Researcher/Sr. Manager with Samsung Research America's Multimedia Standards Research

Lab in Richardson, TX, 2012-2015, Sr. Staff Researcher/Media Analytics Lead with FutureWei (Huawei) Technology's Media Lab in Bridgewater, NJ, 2010-2012, an Assistant Professor with the Dept of Computing, The Hong Kong Polytechnic University from 2008 to 2010, and a Principal Staff Research Engineer with the Multimedia Research Lab (MRL), Motorola Labs, from 2000 to 2008. His research interests include point cloud and light field compression, graph signal processing and deep learning in the next gen visual compression, image processing and understanding. He has 50+ issued or pending patents, 180+ publications in book chapters, journals, and conferences in these areas. He is an IEEE senior member, associate Editor-in-Chief for IEEE Trans on Circuits & System for Video Tech, associated editor for IEEE Trans on Image Processing(2020), IEEE Trans. on Multimedia (2015-18), IEEE Trans on Circuits & System for Video Technology(2016-19). He serves on the steering committee member of IEEE ICME (2015-18), and he is an elected member of the IEEE Multimedia Signal Processing (MMSP), IEEE Image, Video, and Multidimensional Signal Processing (IVMSP), and IEEE Visual Signal Processing & Communication (VSPEC) Tech Committees. He is program co-chair for IEEE Int'l Conf on Multimedia & Expo (ICME) 2019, and co-chaired the IEEE Visual Communication & Image Processing (VCIP) 2017. He received the Best Paper Award at IEEE Int'l Conf on Multimedia & Expo (ICME), Toronto, 2006, and the Best Paper Award (DoCoMo Labs Innovative Paper) at IEEE Int'l Conf on Image Processing (ICIP), San Antonio, 2007.